Advances in Natural Science **ISSN 1715-7862 [PRINT]**
Vol. **3**, No. **2**, **2010**, pp. 235-243 **ISSN 1715-7870 [ONLINE]**
www.cscanada.net **www.cscanada.org**

The 3rd International Conference of Bionic Engineering

Study on Drag Reduction Characteristic Around Bodies of Revolution with Bionic Non-smooth Surface[1]

TIAN L. M.[2]
REN L.Q.[3]
JIANG X.[4]
ZHAO J.N.[5]
ZHANG S.C.[6]
YU S.W.[7]

Abstract: Bionic non-smooth structures on the bodies of revolution had characteristic of drag reduction. In this paper, oil flow visualization test were made in low speed wind tunnel between two bionic non-smooth surface models and smooth surface model. The results show that the oil flow pattern is significantly difference according to the configuration of non-smooth structures, and had obviously effect on the friction of the model. However, the total drag coefficient of BNNS model is reduced. It was found that the BNSS can decrease the pressure drag obviously. The mechanism of BNSS is through sacrifice small viscous force, early flow separation on the blunt body of revolution was restrained, and the pressure force reduced dramatically, so the total force reduced also.
Key words: Oil flow visualization; drag reduction; non-smooth surface; bionic

[1] Key Program of National Natural Science Foundation of China (Grant No.50635030), the International (Regional) Cooperation and Exchange of National Natural Science Foundation of China (Grant No.50920105504), Scientific Research program of Jilin Province (Grant No.20070546), and scientific Forefront and Interdisciplinary innovation project, Jilin University (Grant No. 200903269).

[2] Key Laboratory of Bionics Engineering, Ministry of Education, Jilin University, Changchun, 130025, P .R. China.
[3] Key Laboratory of Bionics Engineering, Ministry of Education, Jilin University, Changchun, 130025, P .R. China.
[4] Jilin Vocational & Technical College Traffic, Changchun, 130022, P .R. China.
[5] FAW-Volkswagen Automotive co., ltd, Changchun,130011,P.R. of China.
[6] ANSY SPera Global, 100000, Beijing, P .R. China.
[7] Jilin Fangtian Pump Manufacture ltd.
*Received 10 April 2010; accepted 18 July 2010

1. INTRODUCTION

In search of improving drag reduction, we were inspired by the variety of non-smooth structures on the skins of living creatures for their excellent drag reduction (LEE & LEE, 2001; Bechert et al., 2000; Bechert et al., 2000; Walsh, 1990). Dung beetles, for example, having many concave domes on their body surface can live in the moist or adhesive soil freely, but the soil seldom sticks to their bodies (REN et al., 2001; REN et al., 1992; QIAN et al., 1992; TONG et al., 1994). The humpback whale flippers, having tubercles on the leading-edge can delay stall by providing higher lift at higher incidence angles, and to ameliorate the poststall characteristics by maintaining higher lift with lower drag (Miklosovic et al., 2004). The cytister bengalensis aube, which was praised as pet of god, can live in the land, the water and sometimes can fly on the air, has dimple concave on the body surface (ZHOU et al., 2006). Not only the animals and insect, but also plants, have non-smooth structures on the skin, such as the leaf of the lotus. Just these kinds of non-smooth structures combining with the epuciticular wax crystalloids made the lotus leaf having the ability of self-cleaning (Barthlott & Neinhuis, 1997). Though there were different configurations on their body surface, they had the same characteristic on their surface, which were the non-smooth surface and the drag reduction. The photo of these samples is shown in Fig.1.These non-smooth structures have been selected naturally for survival. The surface with regular non-smooth structures imitating living creature's skin is called bionic non-smooth surface (BNSS). Inspired by above living creatures, two different BNSS were designed and machine on the bodies revolutions directly. In order to investigate the drag reduction characteristic about BNSS, oil flow visualization test between two BNSS and one smooth surface model were made in low speed wind tunnel.

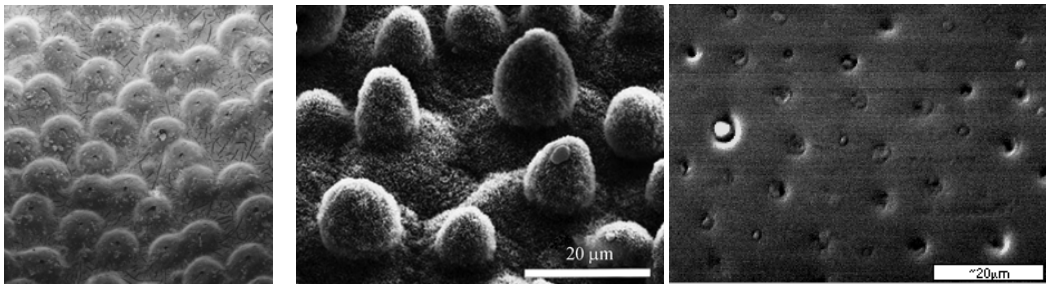

(a) (b) (c)

(a) Convex domes found on dung beetle (REN et al., 2001)
(b) Mastoid and micro-nano composite structure of lotus leaf (Bechert et al., 2000)
(c) The concave structures of Cytister bengalensis Aube (ZHOU et al., 2006)

Fig. 1: The non-smooth structures of some typical living creature' skin

2. EXPERIMENTAL PROCEDURE

2.1 Experiment model design

The experimental model is bodies of revolution, it is shown as figure.2. The non-smooth structures are sculptured on the body surface beginning from the bottom of the body about 50mm, called the tail. At the position of A, B, C, the curvature changed abruptly. The configurations are convex dome and dimple concave, the diameters are 5mm and 3mm, and the heights are 0.5mm and 0.35mm respectively. The convex domes were distributed as rhombus form and the dimple concave were distributed as rectangle form on the tail of bodies of revolution. The convex dome model is called model1, the other model called model2. The arrangement and distributed of non smooth structures on the model just shown as fig.2 (b) and (c). The parameters of non-smooth structures are shown as table1.

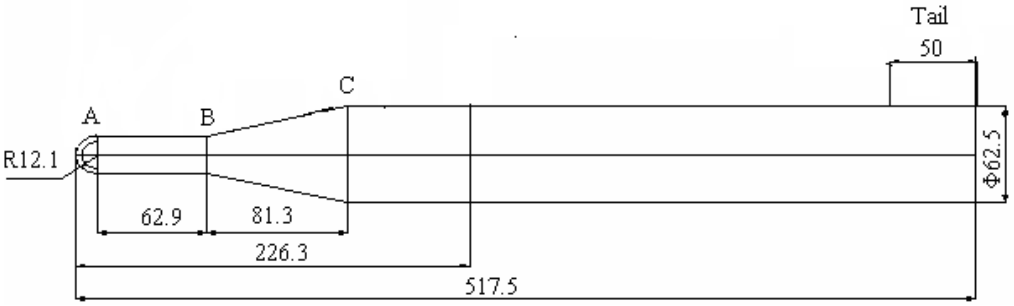

(a) The sketch map of bodies of revolution

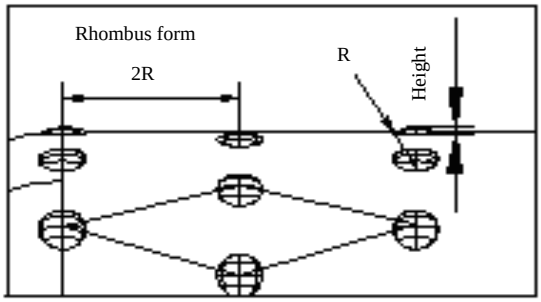

(b) Convex dome non-smooth structures arrangement at rhombus form

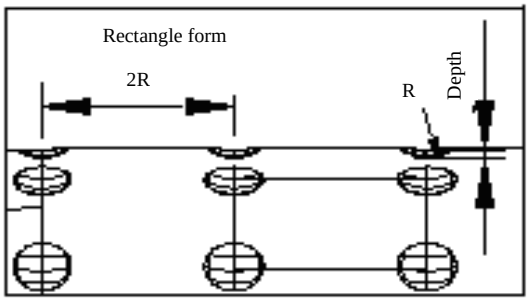

(c) Dimple concave non-smooth structures arrangement as rectangle form

Fig. 2: Different form and arrangement of roughened structure on the bodies of revolution

Table 1: The parameters of non-smooth structure

BNSS model	Form of non-smooth structure	Diameter (mm)	Height/depth(mm)
1	convex dome	5	0.5
2	Dimple concave	3	0.35

2.2 Experimental apparatus and details

Oil flow visualization test were performed in a circulating flow low speed wind tunnel with a testing section of 1 m × 1 m × 1 m. The low speed wind tunnel is shown as fig.3. The turbulence was less than 0.4% and the highest wind speed of tunnel was 60 m/s. The model was placed on the centre of the testing section and connected with mechanical sensors in *x*, *y* and *z* planes through front brackets. At the wind speed of 44m/s, the drag coefficient of smooth surface model and BNSS at low speed wind tunnel was shown as table 2.

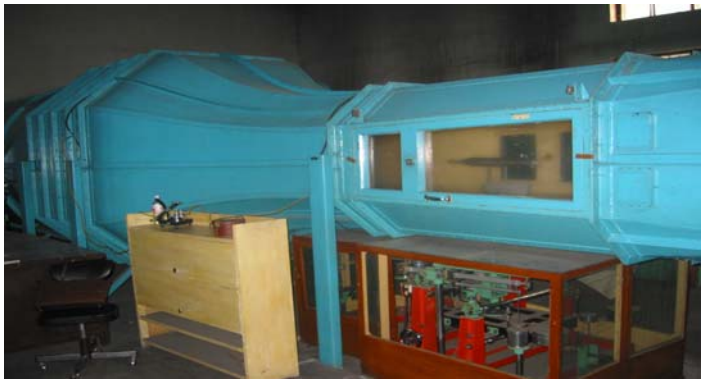

Fig. 3: Low speed wind tunnel with test model in the testing section

Table 2: Drag coefficient of text model in low speed tunnel at wind speed of 44m/s (C_D)

Text model	Smooth model	Convex dome model	Dimple concave model
C_D	0.5757	0.5312	0.5198

2.3 Oil film prepared

2.3.1 Components of oil film

The oil film was composed by oil mixing with small particles powder paint. Oil is kind of carrier, and powder paint is tracer particles. In order to in order to make tracer particles mix with oil more evenly and meanwhile have a better dip together with the model surface, a small amount of additives were added in it.

1) Tracer particles: the experiment was carried through in low speed wind tunnel; the model surface was sprayed by black paint, and therefore, titanium dioxide (TiO2) which has the proportion of 4.0, a molecular weight of 79.90 white powders was chosen as tracer particles.
2) Oil solutions (carrier): the oil viscosity affect the oil flow path line's definition, development time under oil flow shear stress, and the ability to maintain its status after stop the wind tunnel. It is the primary factor to determine the oil flow pattern's quality. So the viscosity is the main consideration when select oil solutions. Oil viscosity is decided by the flow velocity, and in order to obtain moderate viscosity, two or more oil mixed together also can be selected. The wind speed of this experiment is 44m / s; it belongs to low-speed conditions, and chooses mixed kerosene oil as carrier. Various parameters of the selected oils are: silicone oil, molecular is Polydimethylsiloxane oxygen alkanol, Molecular weight is about 2000, kinematic viscosity is 200×10^{-6}m2/s, density is 950kg/m^3, surface tension is 20.6×10^{-5}N/cm. kerosene oil, density no more than 840kg/m^3 at 20 ^{O}C, kinematic viscosity no more than 2.0×10^{-6}m^2/s at 40 ^{O}C, without mechanical impurities and water, no water-soluble acid or alkali, chroma is +19, turbidity point no higher than-15 ^{O}C.
3) Additive: Oleic acid was selected as additives in this test. It may help reduce the condensation, so the tracer particles can distribute evenly in the oil and a uniform film layer is obtained.

2.3.2 Mix ratio of oil film components

Firstly, modulate titanium dioxide and silicone oil with a ration of 1:2 (volume), then dilute with the kerosene, and finally add a small amount of oleic acid. The final confirmed ratio of them through several pre-tests. The film components volume ratio is shown as table3. It is a rough range of proportion, since the daily external environment such as temperature; humidity will impact on the film quality, so it must go through a lot of pre-tests to adjust it until the oil flow patterns are clear.

Table 3: The film components ratio (volume ratio)

Oil film component	Titanium dioxide	silicon oil	kerosene	Oleic acid
Wind speed at 44m/s	5	7	3	15ml/100ml

3. RESULT AND DISCUSSION

Oil flow trochoid (OFT) can denote the frictional stress approximately, through the analysis of oil flow pattern; the whole flow around bodies of revolution characteristic can be obtained. Fig4. is oil pattern of experimental models at the wind speed 44m/s. The overall flow characteristics of all the models are the same, the OFT of all the models nearly parallel the model axes, and all of them appear oil accumulate phenomena at the same position on the effect of flow separation and reattachment. At the position of A, B and C on the model shown as fig.2(a), orbicular oil accumulated area are very obviously. However, the

existence of non-smooth structures had certain influence on the flow field. The oil flow pattern is significantly difference at the tail according to the configuration of non-smooth structures. The non-smooth structure display on the tail of the model had obviously effect on the friction of the model. At the tail of the model, the shearing stress of non-smooth models was higher than smooth surface model. Meanwhile, the width of oil accumulated area is changed.

position A and B position C tail

(a) Different position of smooth surface model

position A and B position C tail

(b) Convex dome distributed on the tail of the model

position A and B position C tail

(c) Dimple concave distributed on the tail of the model

Fig. 4: Oil pattern of experimental models at the wind speed 44m/s

From fig.4, it can be seen the oil flow pattern is significantly difference at the tail according to the configuration of non-smooth structures. Fig.5 (a) is the oil flow pattern of convex dome model at the wind speed is 44m/s and attack angle is 0°. 5(b) is the sketch map of turbulent flow around convex dome. From figure5 it can be seen at the windward side of convex B, there is nearly circle separate line, and there are two approximate symmetry vortexes Fb1 and Fb2 at the leeward side. Meanwhile, convex B had significantly effect on convex D. it made the separation is not very clear at the windward side of convex D, and symmetrical vortex was formed on there, these phenomenon is not appear at the windward side of A, B and C. At the leeward side, two approximate symmetry vortexes Fd1 and Fd2 were formed, the separate line of wake is very clear. However, the convex B had no significantly effect on the convex A and C.

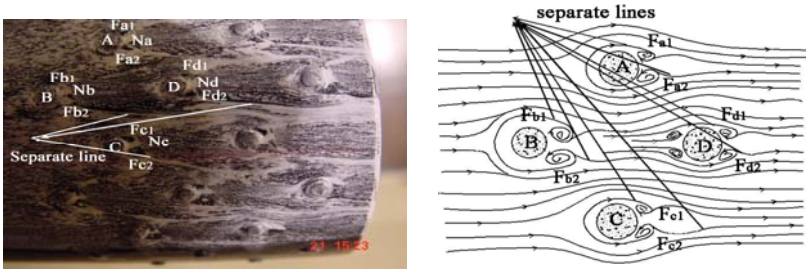

(a) Oil pattern of convex dome **(b) Sketch map of turbulent flow around convex dome**

Fig. 5: Oil pattern at the wind speed is 38m/s and attack angle is 0°

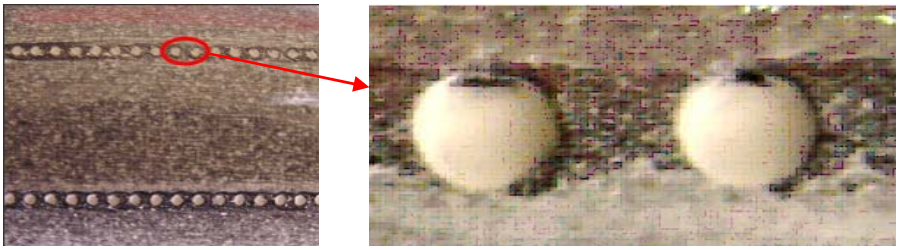

(a) Oil pattern of dimple concave (b) Detail view of oil pattern about dimple concave

Fig. 6: Oil pattern of dimple concave at wind speed is 44m/s, attack angle at 0°

Fig 6 shows the oil flow pattern of dimple concave model, the shear stresses near them are significantly higher than other places. There are stress concentrate strips under the effect of dimple concave non-smooth structures and the width of them nearly equal to the diameter of dimple concave. Oil accumulate phenomena inside dimple concave are very obviously, that means the shear stresses of fluids inside dimple concave are so small that it could not promote the tracer particles move alone the flow. The reason for this situation is because of the stream flow contact with airflow exist in dimple concave, it belongs to gas-gas contact, so the share stress is smaller. However at the back area of dimple concave, the stream flow contact with solid model surface directly, comes in to gas-solid contact, the velocity gradient is larger, so the shear stress increased clearly.

4. THE MECHANISM OF DRAG REDUCTION OF BNSS

From oil pattern of BNNS model show as figure5 and figure6, the viscous drag must higher than smooth surface model. However, table 2 indicated that the total drag of BNNS model is reduced. The only reason of it is the pressure drag reduced significantly. Table4 is the drag coefficient of experimental model through simulation, it validate this hypothesize. The non-smooth structures changed the wake of the BNNS model, so the total force improved greatly.

Table 4: Drag coefficient of experimental model

model	Pressure force coefficient	Viscous force coefficient	Total force coefficient
Smooth surface	0.4181	0.1176	0.5357
Convex dome model	0.3311	0.1496	0.4807
Dimple concave model	0.3337	0.1507	0.4845

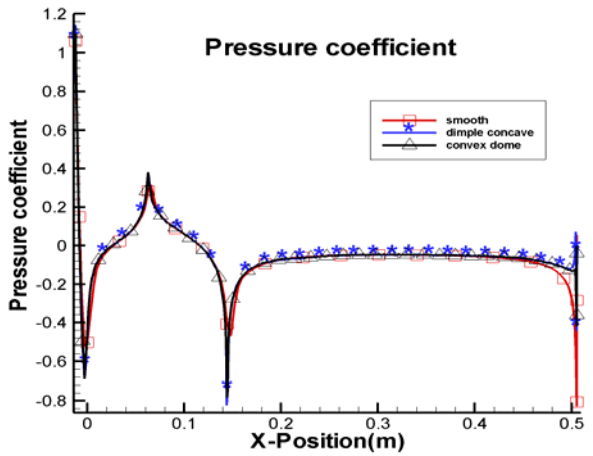

(a) Distributing map of pressure coefficient on x direction

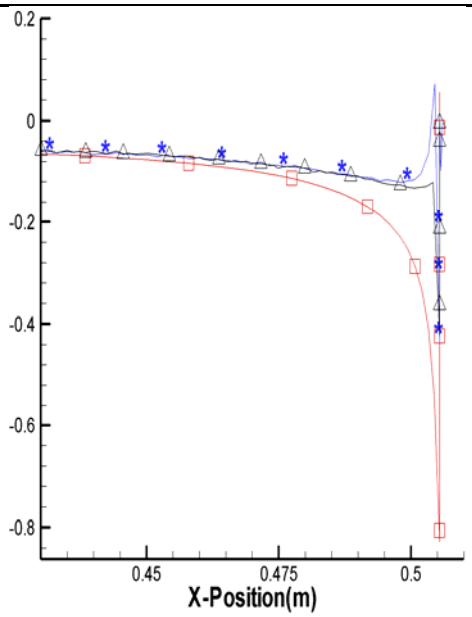

(b) Partial enlarge map of pressure coefficient on the tail

Fig.7: Contrast map of pressure coefficient on x direction between smooth model and non-smooth model

Fig.7 was the contrast map of pressure coefficient on x direction between smooth surface model and non-smooth surface model. The speed of airflow reduced sharply because of block of the head of the model, and the pressure coefficient increased rapidly. At the place which the head connecting with column, pressure reduced notably, it was denoted that the speed of airflow increased distinctly. At the shoulder of the model, the area of section increased abruptly, the speed of airflow increased, it seemed that they would depart from the model and had the trend of separate, so the shearing stress of the shoulder on the model reduced. After that, at the effect of the column of the model, the airflow was attached on the model again, and the pressure coefficient resumed gradually. At about 50mm, the distance from the bottom of the model, the pressure coefficient of smooth surface model reduced sharply. It was denoted that at the tail of the model, the faintish separate had already appeared, so the base drag became increased. However, the non-smooth structure displayed on the tail of the model could disturb turbulence effectively, so the pressure coefficient of non-smooth surface model reduced very slowly. At this condition, the pressure force was brought by the viscosity of air in the boundary layer.Fig.8 was the static pressure isoline of the models; the static pressure coefficient was expressed as the follow,

$$C_p = \frac{(p - p_{ref})}{q_{ref}}$$

and p stands for static pressure, p_{ref} stands for relative static pressure, q_{ref} stands for relative dynamic pressure.(a) (b)(c) of the figure.8 were stand for smooth surface model, convex dome surface model, and dimple concave surface model respectively, every model was displayed 1/4 area of the whole model only. From fig.8, it could be seen that at the center of the model, the static pressure coefficient of both smooth surface model and non-smooth surface models almost the same; however, at the edge of the base of smooth surface model, the static pressure coefficient was lower than other non-smooth surface model obviously. So the base drag of smooth surface model was larger than that about non-smooth surface model. According to the relationship between viscous and pressure force shown as fig9. Through sacrifice small viscous force, spherical crown pressure force can be reduced dramatically on the blunt body of revolution, so the total force also reduced.

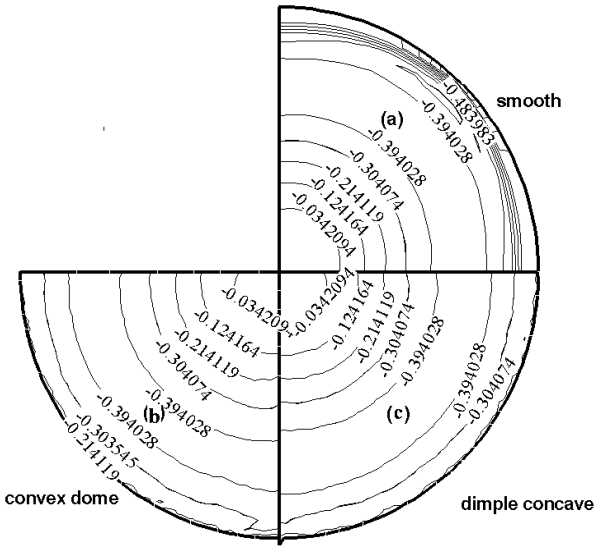

Fig. 8: The static pressure isoline of the model

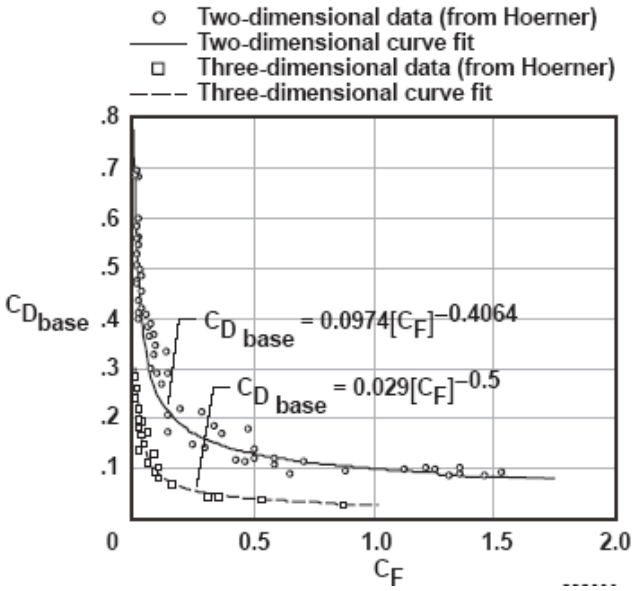

Fig. 9: The relationship between viscous drag and pressure force of body of revolution (Hoerner & Sighard, 1965)

5. CONCLUSION

Compare with smooth surface model, BNSS models changed the oil flow trochoid pattern, and shear stress of BNSS increasing clearly. However, BNSS can decrease the pressure drag significantly. The BNSS utilizing the relationship of viscous and pressure force on blunt body of revolution, through sacrifice small viscous force, early flow separation on the blunt body of revolution was restrained, and pressure force can be reduced dramatically, so the total force reduced also.

REFERENCES

D. S Miklosovic., M. M.Murray, L. E.Howle, and F. E. Fish. (2004). Leading edge tubercles delay stall on humpback whale (Megaptera novaeangliae) flippers. *Physics of Fluids*. *16(5)*: L39-L42

D.W. Bechert, M. Bruse, W. Hage. (2000). Experiments with three-dimensional riblets as an idealized model of shark skin. *Experiments in Fluids. 28*: 403-412.

D.W. Bechert M. Bruse7 W. Hage R. Meyer. (2000). Fluid Mechanics of Biological Surfaces and their Technological Application. *Naturwissenschaften, 87*: 157–171

Hoerner, Sighard F.. (1965). *Fluid-Dynamic Drag: Practical Information on Aerodynamic Drag and Hydrodynamic Resistance*. Self-published work, Library of Congress Card Number 64-19666, Washington, D.C..

M.J.Walsh. Riblets. (1990). In: Bushnell DM, Hefner JN (eds) Viscous drag reduction in boundary layers. *Progress in astronautics and aeronautics, AIAA, Washington. 123*: 203–262.

QIAN C., REN L.Q., CHEN B.C, YAN B.Z.. (1992). Using Characteristics of Burrowing Animals to Reduce Soil-Tool Adhesion. *Transactions of Chinese Ssociety of Aagricutral Engineering*. *46(2)*: 1549-1556.

REN L.Q, TONG J., LI J.Q, CHEN B.C. (2001). Soil Adhesion and Biomimetics of Soil-engaging Components: a Review. *J. agric. Engng Res*. *79 (3)*: 239-263.

REN L.Q,CONG Q., TONG J.. (1992). The study of essential character about non-smooth surface on the interfacial adheresion system. *Agricultural engineering*, *8(1)*:16-22.

S.J. LEE, S.H.LEE. (2001). Flow Field Analysis of a Turbulent Boundary Layer Over a Riblet Surface. *Experiments in Fluids*, *30*: 153-166.

TONG J., REN L.Q, CHEN B.C. (1994). Geometrical morphology Chemical constitution and wettability of body surfaces of soil animals. *International Agricultural Engineering Journa*l, *3(1 and 2)*: 59-68.

W. Barthlott, C. Neinhuis. (1997). Purity of the sacred lotus, or escape from contamination in biological surfaces. *Planta , 202*: 1-8

ZHOU C.H., REN L.Q, ZHANG R., WANG S.J., ZHOU W.F.. (2006). The relationship between the body surface structure of Cybister bengalensis and its unction of reducing resistance. *Journal of Northeast Normal University (Natural Science Edition)(in Chinese), 38*: 109-113.